A Spectrum-Efficient FSK Radar Technology for Range Tracking of Both Moving and Stationary Human Subjects

Jing Wang[®], Student Member, IEEE, Tanja Karp, Senior Member, IEEE,
José-María Muñoz-Ferreras[®], Member, IEEE,
Roberto Gómez-García[®], Senior Member, IEEE,
and Changzhi Li[®], Senior Member, IEEE

Abstract—This article presents a spectrum-efficient frequencyshift keying (FSK) radar technology for Doppler frequencybased moving targets tracking and vital signs (i.e., respiration and heartbeat) based stationary human subject range detection. Fundamental theories of range tracking of linearly moving and periodically moving targets are explained. Different phase extraction methods are categorized and analyzed based on the applicable motion types. The advantage(s), disadvantage(s), and range tracking performance of these methods are compared and summarized. In addition, special conditions and limitations of the different phase extraction techniques are studied. Moreover, range tracking of multiple targets moving in opposite directions and moving in the same direction is investigated. Range detection of a stationary human subject with different orientations relative to the radar line of sight is evaluated. The detection robustness and consistency are explored by measuring a periodically moving small corner reflector at various locations relative to the radar.

Index Terms—Frequency-shift keying (FSK) radar, range tracking, spectrum efficiency, stationary human, vital signs monitoring, wireless sensor.

I. INTRODUCTION

RACKING of both moving and stationary human subjects are of significant interests in both civilian and military applications [1]. Among them, search and rescue of surviving victims immobilized under earthquake rubble or collapsed building debris, hidden intruder detection and tracking [2], and occupancy sensing for heating, ventilation, and air conditioning (HVAC) control [3] are the examples to

Manuscript received April 24, 2019; revised July 18, 2019; accepted August 28, 2019. Date of publication October 3, 2019; date of current version December 27, 2019. This work was supported in part by the National Science Foundation (NSF) under Grant CNS-1718483 and Grant ECCS-1808613. This article is an expanded version from the IEEE MTT-S International Microwave Symposium (IMS 2019), Boston, MA, USA, June 2–7, 2019. (Corresponding author: Jing Wang.)

- J. Wang, T. Karp, and C. Li are with the Department of Electrical and Computer Engineering, Texas Tech University, Lubbock, TX 79409 USA (e-mail: anna.wang@ttu.edu; tanja.karp@ttu.edu; changzhi.li@ttu.edu).
- J.-M. Muñoz-Ferreras and R. Gómez-García are with the Department of Signal Theory and Communications, Polytechnic School, University of Alcalá, 28871 Alcala de Henares, Spain (e-mail: jm.munoz@uah.es; roberto.gomez.garcia@ieee.org).

Color versions of one or more of the figures in this article are available online at http://ieeexplore.ieee.org.

Digital Object Identifier 10.1109/TMTT.2019.2941189

be highlighted. A variety of range tracking technologies have been proposed and investigated in the literature, including optical camera, infrared detector, LIDAR, ultrasonic sensor, and radar. Compared with the rest of the range tracking technologies, wireless radar sensors are attractive for their benefits of better privacy protection, immunity to ambient light and temperature changes, robustness against weather conditions, and the long-range coverage. Among different types of radar systems, wideband radar systems, such as frequency-modulated continuous-wave (FMCW) radar [4] and ultrawideband (UWB) radar [5], can detect the absolute range of moving objects. However, they occupy a large bandwidth which means large interference window with increased probability of jamming to other systems and high operational bandwidth requirements on system components. Furthermore, with the exploding popularity of wireless devices, the radio spectrum has become a scarce commodity in many countries. In particular, the coming Internet of Things (IoT) era aims to connect a great number of objects and devices to the core internet in a wireless manner. Spectrum-efficient sensors are in great demand to cope with the conflict between massive IoT connections and limited spectrum resource [6].

Therefore, this study investigates a wireless narrowband frequency-shift keying (FSK) radar technology, which can estimate the absolute range of both moving and stationary human targets with much less bandwidth requirement than its wideband counterparts. In terms of jamming issues, since FSK radar occupies almost two frequencies constantly, it may also be prone to jamming. In addition, the number of required FSK radar sensors may need to be increased for the longrange coverage while maintaining the desired measurement accuracy, which means more frequency usage and jamming possibilities. In this context, frequency hopping techniques can potentially be employed for minimal signal interference and reduced jamming possibilities at the tradeoff of added system complexity. Since range estimation using FSK radar is based on the phase difference between the two received signals, accurate phase extraction becomes very important for reliable range measurements. Hardware phase demodulation solutions proposed in [7]–[9] rely on either microwave circuits or analog

0018-9480 © 2019 IEEE. Personal use is permitted, but republication/redistribution requires IEEE permission. See http://www.ieee.org/publications_standards/publications/rights/index.html for more information.

components that complicate the system architecture. For software phase extraction approaches, Gu and Lien [10] proposed an in-phase/quadrature (I/Q) trajectory-based complex-domain range detection method using two-tone radar. However, only dc-coupled baseband responses were studied without the consideration of ac-coupled baseband signals, which are more preferable and more commonly used due to their higher system dynamic range. Phase extraction in the time domain and frequency domain was compared in [11] and [12], but only for range tracking of moving targets.

No systematical analysis on different phase extraction techniques and performance evaluation has been given to FSK radar for tracking humans in various situations in the literature. Therefore, in this article, different phase extraction methods are categorized and analyzed based on the applicable motion types, including the time-domain method, frequency-domain method, and complex-domain method. Special conditions and limitations are studied, including the presence of multipath interference, the range distortion issue introduced by the ac-coupling circuit, the motion peak amplitude limitation, and the nulling of the fundamental frequency. The advantage(s), disadvantage(s), and the range tracking performance of the different phase extraction methods are summarized. In the authors' previous studies [13] and [14], only range tracking of a single moving target was demonstrated. In this study, range tracking of multiple human targets, including targets moving in opposite directions and moving in the same direction, is investigated. In addition, while the range detection performance for a stationary human subject was evaluated only along the radar line of sight in the previous study [14], range detection of a stationary human subject with different orientations relative to the radar line of sight is further evaluated to better simulate a practical scenario. Moreover, range detection robustness and consistency in the presence of multipath interference are investigated by measuring a periodically moving actuator at various locations relative to the radar.

The fundamental theories of range tracking of linearly moving and periodically moving targets are explained in Section II. Baseband pre-processing is presented in Section III. Different phase extraction methods are analyzed in Section IV. FSK radar implementation and experiments are discussed in Section V. Finally, conclusions are drawn in Section VI.

II. RANGE TRACKING THEORY

As shown in Fig. 1, in the FSK radar system, two discrete frequencies f_1 and f_2 are transmitted in a shared RF chain at a switching rate of $f_{\rm sqr}$. The frequency shift between the two carriers is usually small, i.e., in the kHz or MHz range, which is represented as $\Delta f = f_2 - f_1$, assuming $f_2 > f_1$. In a direct-conversion quadrature FSK radar system, such as the implemented FSK radar shown in Fig. 2, two discrete signal responses associated with the two carriers exist in both I/Q channels due to the switching mechanism. It should be noted that $f_{\rm sqr}$ should be fast enough so that all motion information is well sampled in spite of the square wave modulation.

The transmit signal can be written as

$$T_k(t) = \text{Re}\{\exp[j(2\pi f_k t + \varphi_{o,k}(t))]\}$$
 (1)

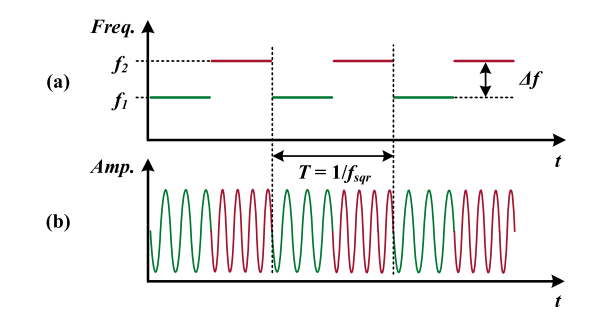


Fig. 1. FSK modulation scheme. (a) Time–frequency representation. (b) Time–amplitude representation.

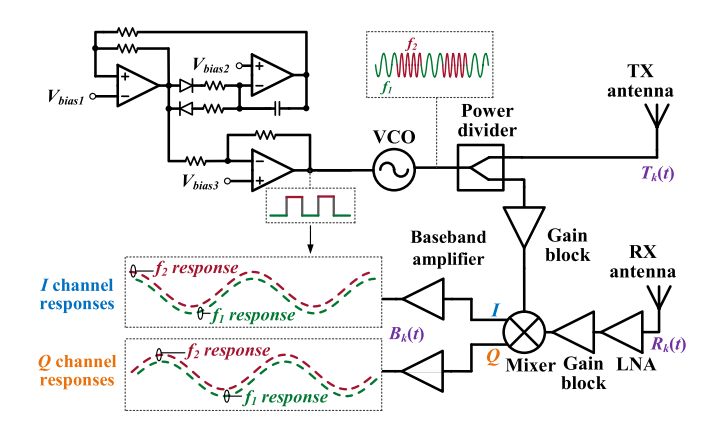


Fig. 2. Block diagram of the implemented FSK radar system.

where k = 1, 2 and $\varphi_{o,k}(t)$ represents the phase noise from the oscillator. Without generality loss, the amplitudes of all signals are normalized to unity. Two different types of motions, i.e., linear motion and periodic motion, typically encountered in indoor human-aware sensing scenarios will be analyzed.

A. Linear Motion

For range-tracking of a linearly moving target, the reflected signal will be shifted in frequency due to the Doppler effect. A phase delay is also generated by the round-trip travel of the signal. The received signal can be approximated as

$$R_{k}(t) \approx \operatorname{Re}\left\{\exp\left[j\left(2\pi\left(f_{k} \pm \frac{2vf_{k}}{c}\right)t - \frac{4\pi R_{0}}{\lambda_{k}}\right) + \varphi_{o,k}\left(t - \frac{2R_{0}}{c}\right) - \varphi_{r,k}\right)\right]\right\}$$

$$= \operatorname{Re}\left\{\exp\left[j\left(2\pi\left(f_{k} \pm f_{d,k}\right)t - \frac{4\pi R_{0}}{\lambda_{k}}\right) + \varphi_{o,k}\left(t - \frac{2R_{0}}{c}\right) - \varphi_{r,k}\right)\right]\right\}$$
(2)

where c is the speed of light, λ_k is the wavelength corresponding to each carrier frequency, R_0 represents the range to target at a particular time $t = t_0$, v is the speed of the target at R_0 , $f_{d,k}$ stands for the generated Doppler frequency, and $\varphi_{r,k}$ denotes the phase delay in the receiver circuit. The difference between $\varphi_{r,1}$ and $\varphi_{r,2}$ is normally small since the two carrier frequencies are very close to each other. Therefore, they will be neglected in the following analysis. After downconverting

the amplified received signals using a copy of the transmitted signals, the baseband complex-valued output is obtained as

$$B_k(t) = \exp\left[j\left(\mp 2\pi f_{d,k}t + \frac{4\pi R_0}{\lambda_k} + \varphi_k\right)\right]$$
(3)

where $\varphi_k = \varphi_{o,k}(t) - \varphi_{o,k}(t - 2R_0/c)$ is the total residual phase accumulated in the circuit. According to the range correlation theory [15], φ_k is very small compared to other phase terms in (3) and hence will be omitted from the analysis. By keeping Δf very small in comparison with f_k , $f_{d,1}$ and $f_{d,2}$ will be almost identical, i.e., $f_{d,1} \approx f_{d,2}$. Therefore, the phase difference between the two baseband signals is

$$\Delta\varphi(t) = \frac{4\pi R_0}{\lambda_2} - \frac{4\pi R_0}{\lambda_1}.\tag{4}$$

Range estimation can be derived accordingly based on this phase difference associated with the Doppler frequencies as

$$R_0 = \frac{c \,\Delta \varphi(t)}{4\pi \,\Delta f}.\tag{5}$$

Multiple targets range detection is possible when their Doppler frequencies can be separated from the Doppler spectra. By tracking the phase difference on the corresponding separated Doppler peak pairs, the associated individual range can be estimated.

B. Periodic Motion

When the target of interest has a periodic small motion $x(t) = m \cdot \sin \omega_0 t$ at a nominal distance D_0 , where m stands for the motion peak amplitude and ω_0 represents the motion frequency component, the radar signal will be reflected back with its phase modulated by the time-varying periodic motion and a constant phase determined by D_0 . The received signal is approximated as

$$R_k(t) \approx \operatorname{Re}\left\{\exp\left[j\left(2\pi f_k t - \frac{4\pi x(t)}{\lambda_k} - \frac{4\pi D_0}{\lambda_k} + \varphi_k\right)\right]\right\}.$$
 (6)

Unlike the linear motion scenario, the acquired baseband signal will be frequency modulated by the periodic motion frequency, which can be represented using spectral analysis [16] as

$$B_k(t) = \exp\left[j\left(\frac{4\pi x(t)}{\lambda_k} + \frac{4\pi D_0}{\lambda_k} + \varphi_k\right)\right]$$
$$= \sum_{n=-\infty}^{\infty} J_n\left(\frac{4\pi m}{\lambda_k}\right) \exp\left[j\left(n\omega_0 t + \frac{4\pi D_0}{\lambda_k} + \varphi_k\right)\right]$$

where J_n is the *n*th-order Bessel function of the first kind. The periodic baseband signal is represented by the sum of a series of sinusoids at harmonic frequencies of the motion frequency (fundamental frequency for n=1) with their amplitudes determined by the corresponding Bessel function and a constant phase determined by the nominal distance D_0 . Fig. 3 draws the Bessel coefficients versus the motion peak amplitude m. The wavelength used is associated with the lower transmit frequency of the implemented 5.8-GHz FSK

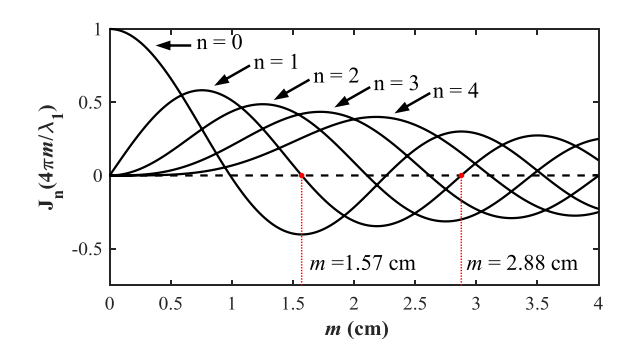


Fig. 3. Bessel coefficients.

radar system, which is $f_1 = 5.822$ GHz. It is shown that the Bessel coefficient of each harmonic frequency component varies with different motion amplitudes. It can even reach zero with certain motion amplitude, which means the corresponding frequency component will vanish from the baseband spectrum. For example, when the motion peak amplitude is 1.57 or 2.88 cm, the corresponding Bessel coefficient equals to zero for the fundamental motion frequency, leading to the nulling of the fundamental frequency. It is not feasible to extract phase information from the motion frequency in this scenario. However, note that the phase difference of any nth-order frequency pair is consistent, which is

$$\Delta\varphi(t) = \frac{4\pi D_0}{\lambda_2} - \frac{4\pi D_0}{\lambda_1}.$$
 (8)

Accordingly, the target range can be estimated based on this phase difference associated with the motion frequency or its harmonics as

$$D_0 = \frac{c \,\Delta \varphi(t)}{4\pi \,\Delta f}.\tag{9}$$

Therefore, the phase difference extraction is not limited to a specific motion frequency pair on the spectrum. To achieve reliable range estimation, the strongest harmonic pairs should be selected due to the corresponding highest signal-to-noise ratio (SNR) when compared to the rest of the frequency pairs. In addition, as shown in (7), phase extraction at the frequency component eliminates the effect of motion displacement. Moreover, if the noise is additive white Gaussian noise (AWGN), its components are distributed across the spectrum. The effect of noise is almost negligible on the frequency peaks on the spectrum. Therefore, phase extraction at the strongest frequency pairs enhances SNR and enables robust nominal distance estimation.

C. Maximum Unambiguous Range

The maximum unambiguous range of an FSK system is limited by the periodicity of the sinusoidal wave [17]. Since $\Delta \varphi(t)$ can only reach a maximum of 2π , range will become aliased beyond this limit. The maximum unambiguous range equation can be derived from (5) and (9) as

$$R_{\text{max}} = \frac{c}{2\Lambda f}.$$
 (10)

Nonetheless, for a given application, the frequency shift can be adjusted to achieve the desired detection range. If high

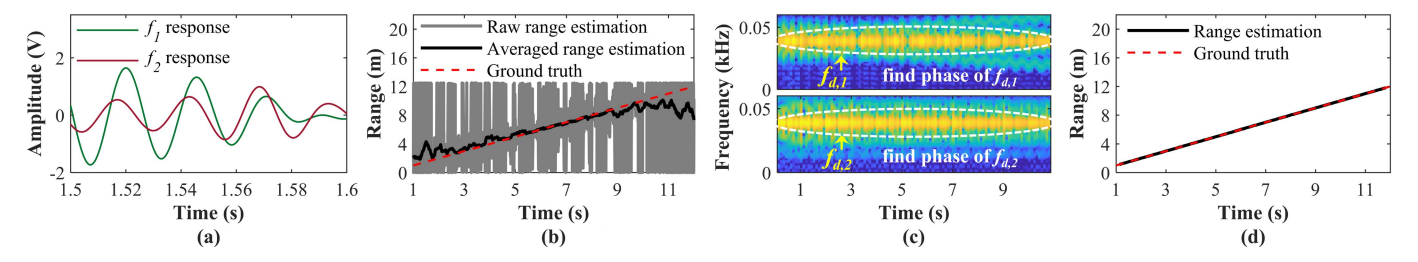


Fig. 4. (a) Simulated *I* channel baseband responses of a linearly moving target in the presence of multipath reflections. (b) Range estimation results using the time-domain method. (c) Spectrograms of the simulated baseband responses. (d) Range estimation results using the frequency-domain method.

measurement accuracy is demanded, other reference systems can be adopted to extend the maximum discernible range without sacrificing the measurement precision. For example, in [18], a hybrid FSK-FMCW system was proposed using an FMCW burst with a small bandwidth to resolve the range ambiguity issue without losing the measurement accuracy. The maximum unambiguous range can also be extended by utilizing more than two carriers [19] or modulating at least one of the carriers.

III. BASEBAND PRE-PROCESSING

As shown in Fig. 2, the square wave control signal is utilized to find the correspondence between the two carriers and their baseband responses. Due to the switching mechanism of FSK modulation, the separated f_1 and f_2 responses are not continuous. In addition, the two responses sample points are not aligned and a phase offset exists between the two carrier responses as a result of this nonsimultaneous transmission. Therefore, if the separated discrete responses are processed directly, the introduced phase offset has to be taken into account and compensated to avoid a bias error in the range measurement [20].

To eliminate the phase offset between the f_1 and f_2 responses and synchronize the sample points, the equivalent continuous baseband responses can be reconstructed using interpolation or filtering. For interpolation-based approaches, data can be directly interpolated to a sufficient number of sample points so that all the useful information are well preserved. The data within each switching section can also be averaged first before performing the interpolation. In this way, the quantization noise caused by the analog-to-digital converter (ADC) and the white noise will be reduced for the measurement data. Nonetheless, the variations caused by the quantization noise and the white noise in the direct interpolation approach can also be reduced later in phase extraction or range estimation stage by applying an average function. The filtering method low-pass filters the baseband response to remove the square wave modulation. An appropriate cutoff frequency between the motion frequency and the square wave frequency need to be chosen to completely remove the square wave modulation with minimum loss of information. These three continuous baseband recovery techniques have a similar amount of computational load and similar performance. In this study, the average-and-interpolation technique is selected to reconstruct the continuous baseband for all the simulations and measurement data henceforth. Data are interpolated with

the same number of sample points as if the associated carrier frequency was transmitted continuously.

IV. PHASE EXTRACTION METHODS

Different phase extraction methods are categorized and summarized according to the applicable motion types. To compare the performance and limitations of the phase extraction methods, range tracking of linear motion and periodic motion were simulated in MATLAB with the same radar settings as the implemented 5.8-GHz radar system used in the experiment of this study, which has $f_1 = 5.822$ GHz, $f_2 = 5.834$ GHz, $f_{\text{sqr}} = 300$ Hz, and a sampling frequency $f_s = 6$ kHz.

A. Linear Motion

A one-way moving target was simulated with a constant speed of 1 m/s and starting distance of 1 m. Since multipath interferences are of primary interest and are more relevant than other factors, such as white noise, multipath reflections were considered in the simulation. Because the undesired indirect path reflections are irregular in urban sensing environment, the simulated multipath reflections were designed to have time-varying amplitudes and random phase delays. The simulated motion signal is around 45 dB above the noise floor on the FFT spectrum for 0.09-s FFT window size and 6-kHz sampling frequency.

1) Time-Domain Method: Fig. 4(a) plots a segment of the simulated *I* channel baseband response with irregular multipath reflections. The instantaneous phase of each carrier response can be acquired directly with respect to time from the complex baseband signal. The corresponding raw range estimation is shown in Fig. 4(b). As can be seen, phase extraction in the time-domain is very sensitive to multipath reflections. Even after applying a 0.25 s moving average filter to the raw range data, some segments of the result are still severely distorted, as shown in Fig. 4(b). In urban sensing environment, the clutter reflections are more complicated than the simulated case. Therefore, the time-domain method may lead to severe distortions and even unacceptable results.

Moreover, the time-domain phase extraction method cannot measure the ranges of multiple targets as the phase terms induced by different targets are inseparable in the time domain of the baseband signals.

2) Frequency-Domain Method: In contrast, the phase can also be obtained in the frequency domain. Short-time Fourier transform (STFT) was performed on the baseband responses

TABLE I Summary of Different Phase Extraction Methods for Range Tracking of Linearly Moving Target

	Time-domain method	Frequency-domain method	
Advantage Simple signal processing		Less sensitive to multipath interferences	
Disadvantage	Very sensitive to multipath interferences	More computation load	
Single target tracking performance	Poor	Good	
Multiple targets tracking capability	No	Yes	

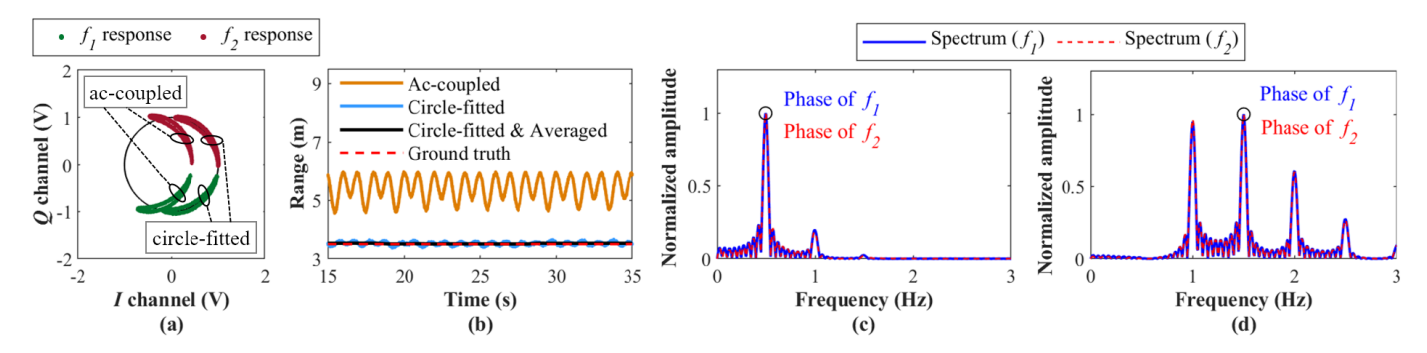


Fig. 5. (a) Simulated ac-coupled baseband response trajectories and corresponding circle-fit trajectories when m=3 mm. (b) Range estimation results using the time-domain method. (c) Spectra of ac-coupled baseband responses when m=2 mm. (d) Spectra of ac-coupled baseband responses when m=1.57 cm.

with a 0.25-s window length and 60% overlap rate to find the Doppler frequency peak on both spectra. The phase comparison was made on the Doppler frequency peak pairs, as shown in Fig. 4(c). Since the STFT provides an integration gain in the Doppler spectrum and can isolate the multipath components that have different frequency signatures than the desired Doppler frequency, this technique operates based on a reliable SNR and enables robust distance estimation, as shown in the range estimation results presented in Fig. 4(d).

In addition, while it is straightforward that the time-domain method can be applied to varying motion speed and irregular moving trajectories, it is worth pointing out that the frequency-domain method also works for such scenarios. Because in frequency-domain method, the target track can be split into many short-time segments, the instantaneous range of each segment can be estimated separately with an inherent tradeoff between the time and frequency resolution due to the Heisenberg uncertainty principle [21]. A summary of the different phase extraction methods for range tracking of linearly moving target is provided in Table I.

B. Periodic Motion

Since the ac-coupled baseband circuit is more commonly used due to its high system dynamic range, ac-coupled baseband responses are considered and analyzed in this study. A digital first-order Butterworth high-pass filter was designed with a cutoff frequency of 0.07 Hz to simulate the behavior of the onboard ac-coupling circuit. AWGN was added to the ac-coupled baseband responses. In this simulation, the motion signal is around 70 dB above the noise floor on the FFT spectrum for 20-s FFT window size and 6-kHz sampling frequency.

1) Complex-Domain Method: A periodic motion was simulated with 0.5-Hz motion frequency and 3-mm motion peak amplitude at a nominal distance of 3.5 m from the radar.

The constellation representation in the complex domain is commonly used for time-varying periodic movement. The simulated baseband response trajectories are plotted in the complex domain in Fig. 5(a). As can be seen, the ac-coupled f_1 and f_2 trajectories are shifted from the unit circle because their dc information are filtered by the ac-coupling circuit. To solve this problem, an analog dc-offset cancellation circuit has been proposed in [22] to automatically remove the dc offset and increase system dynamic range without losing useful dc information. Park et al. [23] proposed an approach for calibrating the undesired dc offset while preserving the useful dc information and obtaining the baseband signal with the maximum resolution. Software techniques have also been proposed to shift the trajectories back to the unit circle, such as circle-fitting [24], which was used in this simulation. The circle-fitted trajectories are shown in Fig. 5(a) as well. After the trajectories are shifted back to the unit circle, range estimation can be acquired by averaging the phase difference of a number of points or finding the angle difference of the shape of the trajectories.

However, the following limitation exists for the complex-domain method. It cannot measure the motion with the amplitude larger than half-wavelength of its carrier frequencies. This is because when the motion peak amplitude exceeds this limit, both trajectories will cover the full unit circle instead of occupying an arc. Hence, there will be no angle difference between them.

2) Time-Domain Method: Similar to linear motion scenario, the instantaneous phase of each carrier response can be obtained directly in the time domain from the complex baseband signal using arctangent demodulation. The difference resides in that the dc components are irrelevant to the desired phase information in linear motion scenario. However, the range-related phase information is carried

	Complex-domain method		Frequency-domain method	
Advantage	Intuitive representation	Intuitive representation No motion amplitude limitation		
Disadvantage	Requires DC offset cancellation; Maximum detectable motion amplitude is limited to half of carrier wavelength	Requires DC offset cancellation	More computation load	
Single target detection performance	Acceptable	Acceptable	Acceptable	
Multiple targets detection capability	No	No	Yes	

TABLE II
SUMMARY OF DIFFERENT PHASE EXTRACTION METHODS FOR RANGE DETECTION OF PERIODICALLY MOVING TARGET

by the dc components of the complex baseband signal in range detection of periodic motion. Therefore, since the dc information of the ac-coupled baseband responses are filtered, the range-related phase information are distorted, as shown from the corresponding range estimation in Fig. 5(b). As discussed with the complex-domain method, circle-fitting was adopted in this simulation to recover the desired dc information and the range estimation was corrected accordingly. However, because of the distortion produced by the accoupling circuit, range variations occur in the corrected range result. Nonetheless, the variation can be efficiently reduced by applying a moving average window, as shown in Fig. 5(b).

3) Frequency-Domain Method: Range estimation of the periodic motion can be realized in the frequency domain as well, which is similar to the linear motion detection except that phase is sought at the motion frequency or its harmonic instead of Doppler frequency. Fig. 5(c) shows the spectra of a 20-s ac-coupled baseband response with AWGN when the motion peak amplitude equals to 2 mm at 2.5 m. In accordance with (7), the motion frequency and its harmonics appear on the spectra. Phase extraction at the frequency peak pairs is less vulnerable to the noise influence because of the integration feature of the applied FFT. The phase response of the on-board first-order high-pass filter is slightly non-linear. However, as shown in (7), since the f_1 and f_2 responses carry exactly the same frequency components except for subtle variations in amplitudes due to different Bessel coefficient, the two carrier responses experience roughly the same phase shift introduced by the high-pass filter. Hence, the phase difference between the baseband responses is almost intact from the phase distortion and the effect on the range estimation is almost negligible. Range estimation of 2.53 m is obtained using (9) from the motion frequency pair with 0.03-m range error, which verifies the insignificant phase distortion effect from the ac-coupling circuit.

A special case example when the peak amplitude causes the Bessel coefficient of the fundamental motion frequency to be zero is shown in Fig. 5(d). Consistent with the plot in Fig. 2, when peak amplitude equals to 1.57 cm at 2.5 m, the amplitude of the baseband component at the motion frequency equals zero, resulting in the nulling of the motion frequency from the spectra. However, according to (7) and (8), any pair of harmonics could be used to produce the range estimation. Since the third harmonic pair has the highest SNR, it is

selected to produce the range estimation. Range of 2.51 m is obtained in this case, which validates the working theory of FSK radar. In this study, the strongest frequency pair is selected regardless of its harmonic order for the frequency-domain method, since it has the highest SNR when compared to the rest of the frequency pairs.

A longer FFT window has a higher integration gain in the spectrum and produces more robust range estimation. However, the resulting low-time resolution may cause impracticality in real-life scenarios. Therefore, the tradeoff between FFT window length and time resolution need to be considered to achieve a balance between reliable measurement and realistic performance. For FFT processing, zero-padding can be used to reduce the picket fence effect [25]. A proper window function should be applied to reduce the inevitable spectral leakage when FFT window length is relatively small [26].

It is also worth specifying that as long as the corresponding frequency components can be successfully detected on the spectra, the frequency and amplitude of the small periodic motion will not affect the detection accuracy of FSK radar. It is possible to detect multiple targets that have different motion frequencies using the frequency-domain method as long as the motion peaks associated with different targets can be separated on the frequency spectra. The summary of the different phase extraction methods for range detection of periodically moving target is provided in Table II.

V. EXPERIMENTS

For range tracking of linear motion, authors in [27] demonstrated the range detection performance of a swaying human subject at three distances using a dual-frequency radar. However, the time-domain phase extraction method was used, yielding very noisy range estimation results. Time-domain and frequency-domain phase extraction methods were compared in [11] by measuring the linear movement of a single and two conducting spheres mounted on linear positioners, respectively. While obvious range variances were observed in the time-domain method, robust range estimation was obtained utilizing the frequency-domain method.

For range detection of periodic motion, one blade covered by the aluminum foil of a three-blade plastic fan was measured by a dual-frequency synthetic aperture radar in [28]. The radar antenna was moved to seven positions forming a synthetic array aperture to estimate the location of the fan blade. However, only the final location result calculated based on the synthetic array processing was provided without demonstrating the performance of each distance measurement that was obtained using a dual-frequency range detection theory. In [10], a two-tone radar was used to measure the mechanical motion of a Newton's cradle at 30 cm. According to the phase difference of the trajectories associated with the two carriers in the complex plane, the range estimation of 30.1 cm was computed. However, only one-time measurement was provided without including results from repeated experiments.

In this study, the range tracking of a single and multiple human subjects in motion was conducted using both the 5.8- and 24-GHz FSK radar. Range detection of a stationary human subject with various orientations relative to the radar line of sight and range detection of a small corner reflector undergoing mechanical periodic motion at different locations relative to the radar were carried out using a 24-GHz FSK radar system. Since the frequency-domain method has proven to be more robust, does not have the motion amplitude limitation, does not require tedious dc offset calibration, and can be applied to both linear and periodic motions compared with the time-domain and complex-domain methods, it was adopted for all of the following conducted experiments.

Fig. 2 shows the block diagram of the designed 5.8-GHz FSK radar system. An operational-amplifier-based circuit is employed to generate a 300-Hz square wave signal, which is used as the control signal of the free-running voltage-controlled oscillator (VCO) to switch between two carrier frequencies f_1 and f_2 . The square wave amplitude levels determine the VCO output frequencies, which are $f_1 = 5.822$ GHz and $f_2 = 5.834$ GHz, with $\Delta f = 12$ MHz. In this case, the maximum unambiguous range is calculated to be 12.4 m. The power splitter divides the carrier signals into two equal parts with one half being transmitted with an average power of 8 dBm while the other half is amplified by a 14-dB gain block and sent to the local oscillator (LO) port of the mixer. The receiver chain consists of an 11-dB low-noise amplifier (LNA) and a 14-dB gain block. Two 2 × 2 patch antennas (one for transmit and one for receive) are used with 11.3-dB gain and 46° half-power beamwidth. Both the square wave and I/Q channels were recorded using NI USB-6009 for all the experiments. The square wave control signal was utilized to separate the f_1 and f_2 responses. Note that to successfully recover phase information and to eliminate the null detection problem (see [29], [30]), the I/Qchannel data were combined to recover the desired motion frequency in the following experiments.

It has been noted that the multipath interference caused by the beam spreading and reflections from the surrounding objects can significantly affect the phase-based range detection performance of the radar system [31]. In a multipath environment, the reflected signals from different pathways combine constructively or destructively with respect to the direct path signal, resulting in a phase-shifted received signal. The phase distortion caused by multipath interference is determined by various factors, such as antenna beamwidth, environment structure, and radar wavelength. While the application environment is beyond control and the effect is difficult to model,

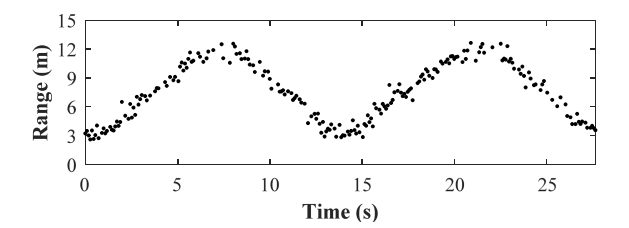


Fig. 6. Range tracking result of a single subject walking back and forth between 2.5 and 11 m in an interior corridor using the 5.8-GHz FSK radar.

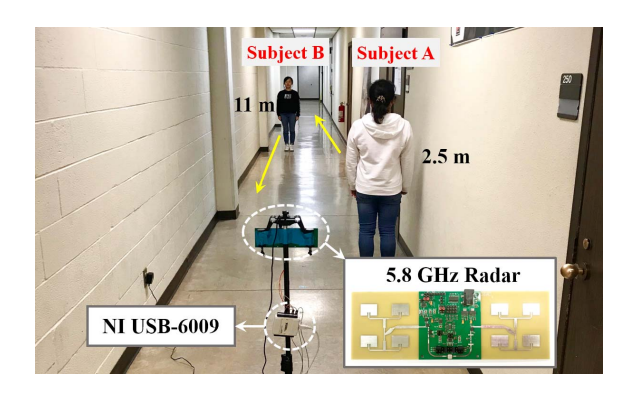


Fig. 7. Photograph of range tracking of two subjects walking in opposite directions in an interior corridor using the 5.8-GHz FSK radar.

narrow antenna beamwidth can effectively reduce the indirect pathways. Considering that the tiny periodic motions are more susceptible to multipath interference than large linear motions, a 24-GHz FSK radar (InnoSent IVS-162) equipped with two 4×2 patch antennas was used for range detection of stationary human subject and range detection of mechanical movement due to its narrower antenna beamwidth than the 5.8-GHz FSK radar that has 2×2 patch antennas.

A. Range-Tracking of Single Moving Human Subject

In this experiment, the 5.8-GHz FSK radar sensor was mounted on a tristand and placed in an interior corridor. To avoid the antenna nearfield and limit the experiment within the maximum unambiguous range, a human subject was asked to complete two round trips from 2.5 to 11 m with a normal walking speed. Measurement data were recorded with 6-kHz sampling frequency. A 0.09-s FFT window length was chosen along with the hamming window and zero-padding. After performing FFT on the separated baseband responses, the Doppler frequencies generated by human walking can be obtained from both frequency spectra. By comparing the phase difference between the two Doppler frequencies, the instantaneous range of the walking subject was estimated according to (5) and shown in Fig. 6.

B. Range-Tracking of Multiple Moving Human Subjects

Range tracking of two subjects walking in opposite directions was carried out in the same environment with the 5.8-GHz FSK radar, as shown in Fig. 7. Subject A walked from 2.5 to 11 m while subject B walked from 11 to 2.5 m. Both started and stopped the movements around the same

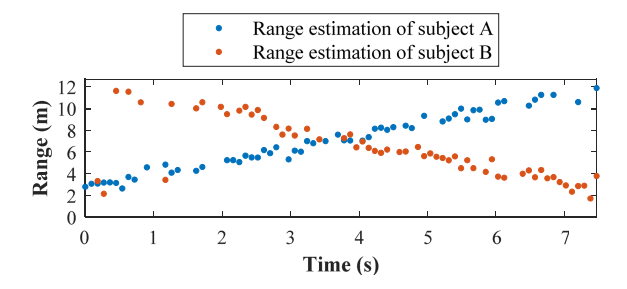


Fig. 8. Range tracking results of two subjects walking in opposite directions in an interior corridor using the 5.8-GHz FSK radar.

time with a normal walking speed. Measurement data were recorded with 6-kHz sampling frequency. The same FFT settings as the single subject tracking experiment were used. The Doppler frequencies generated by the two subjects had opposite signs since the walking directions were opposite. After applying FFT on the baseband responses, the Doppler frequency peaks were successfully separated in the frequency domain and the phase extraction was realized separately on the associated Doppler peaks. Fig. 8 shows the range detection results. It is observed that there are three outlier points at the beginning of the measurement in the walking trajectory of subject B. Because subject A was much closer to the radar than subject B initially, the power of the Doppler frequencies generated by subject A was much higher than that generated by subject B. As a consequence, the Doppler frequencies associated with subject B were buried under the spectral leakage of the Doppler frequencies associated with subject A. Therefore, the phase information of the three outlier points was obtained from the spectral leakage of the Doppler frequencies associated with subject A. This explains why the outliers are located in the trajectory of subject A.

Note that because of multipath interference, the obtained Doppler peaks associated with the two carriers are not always identical to each other. Therefore, in the measurement, only the Doppler peak pairs that were within 1.5-Hz frequency difference were kept and the distorted frequency peaks due to multipath interference were effectively removed.

Compared with the two human subjects moving in opposite directions scenario, the multipath interferences are much more complex for targets moving in the same direction in indoor environments. Therefore, to reduce the effect of multipath interference, range tracking of two human subjects walking in the same direction was performed in an outdoor open area. Because the Doppler frequency is proportional to the carrier frequency, the higher is the carrier frequencies, the more separated the Doppler peaks are and thus, the more accurate the range estimations are. Therefore, the 24-GHz FSK radar was used. A 700-Hz square wave control frequency was generated by an external board, which switched the transmit frequency between 23.8279 and 23.8306 GHz with a frequency shift of 2.7 MHz. The maximum unambiguous range is calculated as 55.5 m. In the experiment, both subjects started the movements around the same time with one subject walking slower than the other. The slower-moving subject walked from 2.5 to 8 m while the faster-moving subject walked from 2.5 to 12 m.

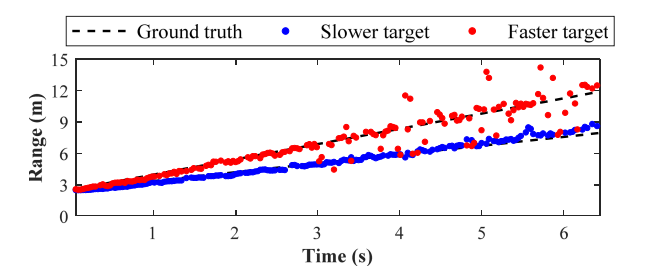


Fig. 9. Range tracking results of two subjects walking in the same direction in an outdoor open area using the 24-GHz FSK radar.



Fig. 10. Photographs of range detection of a seated human subject with different orientations relative to the radar line of sight in an interior corridor using the 24-GHz FSK radar.

Measurement data were recorded with 15-kHz sampling frequency. The recorded data were processed with 0.1-s FFT window size and 0.03-s sliding step along with the hamming window and zero-padding. The frequency tolerance was set at 0.9 Hz, which means that only the Doppler peak pairs within 0.9-Hz frequency difference were processed. As shown in Fig. 9, the tracking results agreed well with the ground truth in the first 3 s. Later, the tracking performance of the faster-moving target degraded due to the low receiving power strength and spectral leakage from the slower-moving target. Overall, the 24-GHz FSK radar has demonstrated acceptable multi-targets tracking performance in an outdoor open area.

C. Range Detection of Stationary Human Subject

Stationary human subject detection experiment was conducted with the 24-GHz FSK radar in the interior corridor. The transmit frequencies were 23.8485 and 23.8650 GHz with a 300-Hz switching frequency generated by a function generator. The maximum unambiguous range is calculated as 9.1 m. Photographs of the experimental setup are shown in Fig. 10. A seated human subject was asked to breathe normally during the measurement time period of 60 s. Three measurements were recorded with 6-kHz sampling frequency at around 1.5 m when the human subject was directly facing the radar, 45° from the line of sight, and -45° from the line of sight, respectively. By comparing the phase difference between the detected respiration tones on both spectra, the absolute distance of the subject was estimated. A 20 s FFT sliding window was used with a 5-s step size. Nine range estimations

TABLE III

AVERAGE RANGE ERROR/STANDARD DEVIATION RESULTS[#] OF RANGE
DETECTION OF A STATIONARY HUMAN SUBJECT FACING DIFFERENT
ORIENTATIONS RELATIVE TO THE RADAR

Meas.*	0 °	45°	-45°
Meas. 1	0.23 / 0.08	0.03 / 0.06	0.13 / 0.11
Meas. 2	0.03 / 0.08	0.06 / 0.12	-0.08 / 0.08
Meas. 3	-0.04 / 0.07	0.03 / 0.07	0.35 / 0.12

[#]The unit of the results is m.

TABLE IV

AVERAGE RANGE ERROR RESULTS[#] OF RANGE DETECTION OF A
PERIODICALLY MOVING ACTUATOR AT VARIOUS LOCATIONS

Meas.*	1 m	1.5 m	2 m	2.5 m	3 m	3.5 m	4 m
Meas. 1	0.25	0.14	0.40	0.06	0.38	0.06	-0.10
Meas. 2	0.09	0.29	0.33	0.02	0.35	0.06	-0.17
Meas. 3	0.12	0.31	0.27	0.04	0.25	0.12	-0.05

[&]quot;The unit of the results is m.

were obtained for each measurement. The range error was calculated as the difference between the average of the nine range estimations and the ground truth. Range error and standard deviation results for the three measurements are listed in Table III.

Approximately, 78% of the range errors were within $\pm 10\%$ of the ground truth, except for the 0.23-m error measured at 0° and the 0.35-m error measured at -45° . Through extensive experimentation, it was revealed that multipath interference was likely the main contribution to the range fluctuation among other possible error sources including frequency drift [32], I/Q channel mismatch [33], [34], and effect of antenna directivity. Nevertheless, the results have demonstrated acceptable accuracy of using FSK technology to detect the range of a stationary human subject based on the vital signs.

D. Range Detection of Mechanical Movement

To further verify the detection consistency and robustness, range detection of a periodic mechanical motion at various locations was carried out in the interior corridor. An actuator (Zaber TSB60-I) mounted with a small triangular trihedral corner reflector (edge length 11 cm) as the target was set with a motion frequency of 0.5 Hz and peak amplitude of 2 mm. Three measurements were recorded with 6-kHz sampling frequency at each location with a 60-s recording length. Data were processed by a 25-s FFT sliding window with a 5-s sliding step size, resulting in eight range estimations for each measurement. Range error was calculated the same way as in the previous experiment and reported in Table IV. The standard deviations of all the measurements were less than 3 cm. Again, multipath interference was deemed to be the major error source. Even though the range error has some fluctuations at different locations, the overall range detection accuracy is acceptable with the largest measured

error being 0.4 m, which equals to 12.7% of the ground truth and 4.4% of the maximum unambiguous range.

VI. CONCLUSION

A spectrum-efficient FSK technology for both moving and stationary human subjects tracking is presented in this article. Fundamental theories of the range tracking mechanisms were explained. Different phase extraction methods were compared and summarized for both linear and periodic motion range detection. In addition, range tracking of both single and multiple moving human subjects was investigated using both 5.8- and 24-GHz FSK radar. Range detection of a stationary human subject facing different orientations and an actuator at various locations has demonstrated acceptable accuracy. Future study will analyze and minimize the error contributions due to multipath, frequency drift, and I/Q channel mismatch.

REFERENCES

- [1] C. Li et al., "A review on recent progress of portable short-range noncontact microwave radar systems," *IEEE Trans. Microw. Theory Techn.*, vol. 65, no. 5, pp. 1692–1706, May 2017.
- [2] V. M. Lubecke, O. Boric-Lubecke, A. Host-Madsen, and A. E. Fathy, "Through-the-wall radar life detection and monitoring," in *IEEE MTT-S Int. Microw. Symp. Dig.*, Honolulu, HI, USA, Jun. 2007, pp. 769–772.
- [3] E. Yavari, C. Song, V. Lubecke, and O. Boric-Lubecke, "Is there anybody in there?: Intelligent radar occupancy sensors," *IEEE Microw. Mag.*, vol. 15, no. 2, pp. 57–64, Mar./Apr. 2014.
- [4] Z. Peng et al., "A portable FMCW interferometry radar with programmable low-IF architecture for localization, ISAR imaging, and vital sign tracking," *IEEE Trans. Microw. Theory Techn.*, vol. 65, no. 4, pp. 1334–1344, Apr. 2017.
- [5] J. Wang, Y. Tang, J.-M. Muñoz-Ferreras, R. Gómez-García, and C. Li, "An improved indoor localization solution using a hybrid UWB-Doppler system with Kalman filter," in *Proc. IEEE Radio Wireless Symp. (RWS)*, Anaheim, CA, USA, Jan. 2018, pp. 181–183.
- [6] L. Zhang, Y.-C. Liang, and M. Xiao, "Spectrum sharing for Internet of Things: A survey," *IEEE Wireless Commun.*, vol. 26, no. 3, pp. 132–139, Jun. 2019.
- [7] S. Lindner, F. Barbon, S. Mann, G. Vinci, R. Weigel, and A. Koelpin, "Dual tone approach for unambiguous six-port based interferometric distance measurements," in *IEEE MTT-S Int. Microw. Symp. Dig.*, Seattle, WA, USA, Jun. 2013, pp. 1–4.
- [8] S. Lindner, F. Barbon, S. Linz, S. Mann, R. Weigel, and A. Koelpin, "Distance measurements based on guided wave 24GHz dual tone sixport radar," in *Proc. 11th Eur. Conf. Radar*, Oct. 2014, pp. 57–60.
- [9] K. Haddadi and T. Lasri, "V-band two-tone continuous wave radar operating in monostatic/bistatic mode," in *Proc. 9th Eur. Conf. Radar*, Amsterdam, The Netherlands, Oct./Nov. 201, pp. 266–269.
- [10] C. Gu and J. Lien, "A two-tone radar sensor for concurrent detection of absolute distance and relative movement for gesture sensing," *IEEE Sensors Lett.*, vol. 1, no. 3, Jun. 2017, Art. no. 3500504.
- [11] Y. Zhang, M. Amin, and F. Ahmad, "A novel approach for multiple moving target localization using dual-frequency radars and time-frequency distributions," in *Proc. 41st Asilomar Conf. Signals, Syst. Comput.*, Pacific Grove, CA, USA, Nov. 2007, pp. 1817–1821.
- [12] Y. Zhang, M. Amin, and F. Ahmad, "Time-frequency analysis for the localization of multiple moving targets using dual-frequency radars," *IEEE Signal Process. Lett.*, vol. 15, pp. 777–780, Nov. 2008.
- [13] J. Wang and C. Li, "A human tracking and physiological monitoring FSK technology for single senior at home care," in *Proc. 40th Annu. Int. Conf. IEEE Eng. Med. Biol. Soc. (EMBC)*, Honolulu, HI, USA, Jul. 2018, pp. 4432–4435.
- [14] J. Wang, T. Karp, J.-M. Muñoz-Ferreras, R. Gómez-García, and C. Li, "A spectrum-efficient FSK radar solution for stationary human subject localization based on vital sign signals," in *IEEE MTT-S Int. Microw. Symp. Dig.*, Boston, MA, USA, Jun. 2019, pp. 140–143.

^{*}Meas. represents measurement.

^{*}Meas. represents measurement.

- [15] A. D. Droitcour, O. Boric-Lubecke, V. M. Lubecke, J. Lin, and G. T. A. Kovacs, "Range correlation and I/Q performance benefits in single-chip silicon Doppler radars for noncontact cardiopulmonary monitoring," *IEEE Trans. Microw. Theory Techn.*, vol. 52, no. 3, pp. 838–848, Mar. 2004.
- [16] C. Li, Y. Xiao, and J. Lin, "Experiment and spectral analysis of a low-power Ka-band heartbeat detector measuring from four sides of a human body," *IEEE Trans. Microw. Theory Techn.*, vol. 54, no. 12, pp. 4464–4471, Dec. 2006.
- [17] M. I. Skolnik, Introduction to Radar Systems. Columbus, NY, USA: McGraw-Hill, 1980.
- [18] J. Wang, Z. Peng, and C. Li, "An efficient and extended range tracking method using a hybrid FSK-FMCW system," in *IEEE MTT-S Int. Microw. Symp. Dig.*, Chengdu, China, May 2018, pp. 1–4.
- [19] H. Zhang and K. Wu, "Three-frequency principle for automotive radar system," in *Proc. IEEE Radio Wireless Conf.*, Atlanta, GA, USA, Sep. 2004, pp. 315–318.
- [20] J.-M. Muñoz-Ferreras, J. Wang, T. Zhou, R. Gomez-Garcia, C. Li, and L. Ran, "Accuracy improvement in range measurements of short-range FSK radars," in *IEEE MTT-S Int. Microw. Symp. Dig.*, Chengdu, China, May 2018, pp. 1–4.
- [21] L. Cohen, Time-Frequency Analysis. Englewood Cliffs, NJ, USA: Prentice-Hall, 1995.
- [22] D. Tang, J. Wang, W. Hu, Z. Peng, Y.-C. Chiang, and C. Li, "A DC-coupled high dynamic range biomedical radar sensor with fast-settling analog DC offset cancelation," *IEEE Trans. Instrum. Meas.*, vol. 68, no. 5, pp. 1441–1450, May 2019.
- [23] B.-K. Park, O. Boric-Lubecke, and V. M. Lubecke, "Arctangent demodulation with DC offset compensation in quadrature Doppler radar receiver systems," *IEEE Trans. Microw. Theory Techn.*, vol. 55, no. 5, pp. 1073–1079, May 2007.
- [24] S. Guan, J. A. Rice, C. Li, and C. Gu, "Automated DC offset calibration strategy for structural health monitoring based on portable CW radar sensor," *IEEE Trans. Instrum. Meas.*, vol. 63, no. 12, pp. 3111–3118, Dec. 2014
- [25] A. A. Girgis and F. M. Ham, "A quantitative study of pitfalls in the FFT," *IEEE Trans. Aerosp. Electron. Syst.*, vol. AES-16, no. 4, pp. 434–439, Jul. 1980.
- [26] R. Lyons, Understanding Digital Signal Processing, 2nd ed. Upper Saddle River, NJ, USA: Prentice-Hall, 2004, pp. 481–482.
- [27] M. Amin, P. Zemany, P. Setlur, and F. Ahmad, "Moving target localization for indoor imaging using dual frequency CW radars," in *Proc.* 4th IEEE Workshop Sensor Array Multichannel Process., Waltham, MA, USA, Jul. 2006, pp. 367–371.
- [28] Y. Zhang, M. Amin, and F. Ahmad, "Localization of inanimate moving targets using dual-frequency synthetic aperture radar and time-frequency analysis," in *Proc. IEEE Int. Geosci. Remote Sens. Symp. (IGARSS)*, Boston, MA, USA, Jul. 2008, pp. II-33–II-36.
- [29] B.-W. Park, S. Yamada, O. Boric-Lubecke, and V. Lubecke, "Single-channel receiver limitations in Doppler radar measurements of periodic motion," in *Proc. IEEE Radio Wireless Symp.*, San Diego, CA, USA, Oct. 2006, pp. 99–102.
- [30] C. Li, V. M. Lubecke, O. Boric-Lubecke, and J. Lin, "A review on recent advances in Doppler radar sensors for noncontact healthcare monitoring," *IEEE Trans. Microw. Theory Techn.*, vol. 61, no. 5, pp. 2046–2060, May 2013.
- [31] S. L. Wilson and B. D. Carlson, "Radar detection in multipath," IEE Proc.-Radar, Sonar Navigat., vol. 146, no. 1, pp. 45–54, Feb. 1999.
- [32] F. Ahmad, M. G. Amin, and P. D. Zemany, "Dual-frequency radars for target localization in urban sensing," *IEEE Trans. Aerosp. Electron. Syst.*, vol. 45, no. 4, pp. 1598–1609, Oct. 2009.
- [33] A. Singh *et al.*, "Data-based quadrature imbalance compensation for a CW Doppler radar system," *IEEE Trans. Microw. Theory Techn.*, vol. 61, no. 4, pp. 1718–1724, Apr. 2013.
- [34] F. Ahmad, M. G. Amin, and P. D. Zemany, "Performance analysis of dual-frequency CW radars for motion detection and ranging in urban sensing applications," in *Proc. SPIE Symp. Defense Secur.*, Orlando, FL, USA, vol. 6547, May 2007.
- [35] Y. Yan, C. Li, and J. Lin, "Effects of I/Q mismatch on measurement of periodic movement using a Doppler radar sensor," in *Proc. IEEE Radio Wireless Symp. (RWS)*, New Orleans, LA, USA, Jan. 2010, pp. 196–199.



Jing Wang (S'16) received the B.S. degree in communication engineering from the Fujian University of Technology, Fuzhou, China, in 2015. She is currently pursuing the Ph.D. degree in electrical engineering at Texas Tech University, Lubbock, TX USA

Her current research interests include microwave circuits, wireless RF sensors, and their biomedical applications.



Tanja Karp (M'97–SM'08) received the Dipl.-Ing. (M.S.E.E.) degree in electrical engineering and the Dr.-Ing. (Ph.D.) degree from the Hamburg University of Technology, Hamburg, Germany, in 1993 and 1997, respectively.

In 1997, she joined the Institute of Computer Engineering, Mannheim University, Mannheim, Germany, as a Senior Research and Teaching Associate. From 1998 to 1999, she was a Guest Lecturer with the Institute for Microsystems Technology, Freiburg University, Freiburg, Germany. From

2000 to 2006, she was an Assistant Professor with the Department of Electrical and Computer Engineering, Texas Tech University, Lubbock, TX, USA, where she is currently an Associate Professor. From 2016 to 2017, she was a U.S. Fulbright Scholar with the University of South Africa (UNISA), Pretoria, South Africa. She has organized several K–12 robotics programs to promote STEM careers. Her current research interests include multirate signal processing, filter banks, multicarrier modulation, and engineering education.

Dr. Karp was a recipient of the IEEE/ASEE Harriet B. Rigas Award in 2012 and the President's Awards for Excellence in Science, Mathematics, Engineering Mentoring (PAESMEM, 2016).



José-María Muñoz-Ferreras (M'15) was born in Madrid, Spain, in 1981. He received the M.Sc. degree in telecommunication engineering and the Ph.D. degree in electrical and electronic engineering from the Polytechnic University of Madrid, Madrid, Spain, in 2004 and 2008, respectively.

He is currently an Associate Professor with the Department of Signal Theory and Communications, University of Alcalá, Alcalá de Henares, Spain. His current research interests include radar signal processing, advanced radar systems and concepts,

and microwave/RF circuits and systems, especially high-resolution inverse synthetic aperture radar images, and the design and validation of radar systems for short-range applications.

Dr. Muñoz-Ferreras is a member of the Technical Review Board of the IEEE International Geoscience and Remote Sensing Symposium, the IEEE Radar Conference, and the European Radar Conference. He is a Reviewer for several IEEE and IET publications.



Roberto Gómez-García (S'02–M'06–SM'11) was born in Madrid, Spain, in 1977. He received the M.Sc. degree in telecommunication engineering and the Ph.D. degree in electrical and electronic engineering from the Polytechnic University of Madrid, Madrid, in 2001 and 2006, respectively.

He has been, for several research stays, with the C2S2 Department, XLIM Research Institute, University of Limoges, Limoges, France, the Telecommunications Institute, University of Aveiro, Aveiro, Portugal, the U.S. Naval Research

Laboratory, Microwave Technology Branch, Washington, DC, USA, and Purdue University, West Lafayette, IN, USA. Since 2006, he has been an Associate Professor with the Department of Signal Theory and Communications, University of Alcalá, Alcalá de Henares, Madrid. He is also an Adjunct Part-Time Professor with the University of Electronic Science and Technology of China, Chengdu, China, and has also been an Invited Visiting Professor with Gdansk University of Technology, Gdansk, Poland since 2018. He has authored or coauthored more than 90 journal articles

(70 in IEEE journals and 35 as first author) and 135 conference articles. His current research interests include the design of fixed/tunable high-frequency filters and multiplexers in planar, hybrid, and monolithic microwave-integrated circuit technologies, multifunction circuits and systems, and software-defined radio and radar architectures for telecommunications, remote sensing, and biomedical applications.

Dr. Gómez-García is a member of the Technical Review Board for several IEEE and EuMA conferences. He is also a member of the IEEE Microwave Theory and Techniques Society (MTT-S) Microwave Acoustics (MTT-2), IEEE MTT-S Filters and Passive Components (MTT-8), the IEEE MTT-S Biological Effects and Medical Applications of RF and Microwave (MTT-10), the IEEE MTT-S Wireless Communications (MTT-20), and the IEEE CAS-S Analog Signal Processing Technical Committees. He was a recipient of the 2016 IEEE MTT-S Outstanding Young Engineer Award. He was an Associate Editor of the IEEE TRANSACTIONS ON MICROWAVE THEORY AND TECH-NIQUES from 2012 to 2016 and the IEEE TRANSACTIONS ON CIRCUITS AND SYSTEMS-I: REGULAR PAPERS from 2012 to 2015, a Senior Editor of the IEEE JOURNAL ON EMERGING AND SELECTED TOPICS IN CIRCUITS AND SYSTEMS from 2016 to 2017, and a Guest Editor of the 2013 and 2018 IEEE JOURNAL ON EMERGING AND SELECTED TOPICS IN CIRCUITS AND SYSTEMS Special Issue on Advanced Circuits and Systems for CR/SDR Applications and Special Issue on Wireless Sensing Circuits and Systems for Healthcare and Biomedical Applications, the IET Microwaves, Antennas, and Propagation 2013 Special Issue on Advanced Tunable/Reconfigurable and Multi-Function RF/Microwave Filtering Devices, IEEE Microwave Magazine 2014 Special Issue on Recent Trends on RF/Microwave Tunable Filter Design and 2019 Special Issue on Wireless Sensors for Biomedical Applications, and the IEEE TRANSACTIONS ON MICROWAVE THEORY AND TECHNIQUES Special Issue on 2019 Radio and Wireless Week. He is currently an Associate Editor of the IEEE JOURNAL OF ELECTROMAGNETICS, RF AND MICROWAVES IN MEDICINE AND BIOLOGY, IEEE ACCESS, the IET Microwaves, Antennas, and Propagation, and the International Journal of Microwave and Wireless Technologies. He is also a Reviewer for several IEEE, IET, EuMA, and Wiley journals.



Changzhi Li (S'06–M'09–SM'13) received the B.S. degree in electrical engineering from Zhejiang University, Hangzhou, China, in 2004, and the Ph.D. degree in electrical engineering from the University of Florida, Gainesville, FL, USA, in 2009.

From 2007 to 2009, he was with Alereon Inc., Ausitn, TX, USA, and then with Coherent Logix Inc., Austin, TX, USA, where he was involved in ultrawideband (UWB) transceivers and software-defined radio, respectively. In 2009, he joined Texas Tech University, Lubbock, TX, USA, as an Assistant

Professor and then became an Associate Professor in 2014. His current research interests include biomedical applications of microwave technology, wireless sensors, and RF/analog circuits.

Dr. Li was a recipient of the IEEE Microwave Theory and Techniques Society (MTT-S) Outstanding Young Engineer Award, the IEEE Sensors Council Early Career Technical Achievement Award, the ASEE Frederick Emmons Terman Award, the IEEE-HKN Outstanding Young Professional Award, the NSF Faculty Early CAREER Award, and the IEEE MTT-S Graduate Fellowship Award. He is an Associate Editor of the IEEE TRANSACTIONS ON MICROWAVE THEORY AND TECHNIQUES, the IEEE TRANSACTIONS ON CIRCUITS AND SYSTEMS—I: REGULAR PAPERS, and the IEEE JOURNAL OF ELECTROMAGNETICS, RF AND MICROWAVES IN MEDICINE AND BIOLOGY. He served as an Associate Editor for the IEEE TRANSACTIONS ON CIRCUITS AND SYSTEMS—II: BRIEFS from 2014 to 2015. He served as a TPC Co-Chair for the IEEE MTT-S International Microwave Biomedical Conference from 2018 to 2019 and the IEEE Wireless and Microwave Technology Conference from 2012 to 2013.